Desalination and Water Treatment
www.deswater.com

doi: 10.5004/dwt.2018.22042

108 (2018) 189–197
March

Characterization of biochars from a plant biomass and its effect on lead sorption capacity

Noeline B. Fernandez*, Manohar D. Mullassery, Diana Thomas, Surya R., Jelen Das Y.

Department of Chemistry, Fatima Mata National College, Kollam 691001, India, emails: fernandeznoeline@gmail.com (N.B. Fernandez), mdmullassery@gmail.com (M.D. Mullassery), dayanathms202@gmail.com (D. Thomas), suryar864@gmail.com (Surya R.), jelenjalano7@gmail.com (Jelen Das Y)

Received 9 August 2017; Accepted 12 February 2018

ABSTRACT

The properties of biochar produced by the pyrolysis of a plant biomass in the temperature range (200°C–500°C), for varying time was analyzed in the present work. The biochar was characterized using FTIR, ^{13}C nuclear magnetic resonance, X-ray diffraction and SEM. Elemental analysis was also carried out to estimate the degree of charring at the various stages. The surface area obtained by Brunauer, Emmett and Teller analysis (1.02–7.97 $m^2 g^{-1}$) showed that fine micropores were developed on the biochar surface. The applicability of the char for heavy metal adsorption from aqueous system was also studied. Langmuir and Freundlich adsorption isotherm models were fitted to the experimental data. From the regression analysis, Freundlich was found to be the best fit model suggesting multilayer adsorption.

Keywords: Biochar; Adsorption; Isotherm models; Kinetics

1. Introduction

Plant biomass–derived char is gaining much importance recently as a potential soil amendment. The immobilization of toxic chemicals in aqueous media and controlled nutrient release are some of the main focus areas in biochar studies. The behaviour of biochar greatly depends on the formation conditions. As already reported by Keiluweit et al. [1], no well-defined structure exists for biochar. Depending on the time and temperature, the char obtained possesses varying degrees of aromaticity and elemental content [2,3]. It is, henceforth, very essential to choose biochars with desired properties for particular application. Therefore, a precise understanding of the structure of the biochar is crucial in understanding the biochar-controlled processes.

Heavy metals, irrespective of their low concentrations in the ground water, are posing great threat to mankind [1,2]. Severe contamination of ground water with heavy metals such as lead, chromium and cadmium has been reported from various parts of the world [4]. The WHO has set a tolerance limit of 5 μg L^{-1} for Pb^{2+} ions in drinking water. Among the possible removal techniques of heavy metals, adsorption is accepted as a quantitative, economic and efficient method [5–7]. A number of researchers have concentrated on fabricating suitable adsorbents for heavy metal retention and removal from wastewaters [8–11]. Biochar and activated carbon find immense application in heavy metal remediation from aqueous systems [11,12,13]. The specific surface area and porosity of the adsorbent significantly influence the adsorption process [14,15]. The extent of lignin and cellulose components in the plant biomass is directly linked to the porosity of the developed biochar [3,4]. Moreover, the presence of oxygen functional groups in the solid matrix and pore surface of the biochar enhances the adsorption process both on the outer surface and the inner pore volume [5,16].

Developing adsorbents for heavy metal remediation is never losing its significance, as the water bodies are continuously getting polluted by industrial effluents. Biochar is significant in the sense that it is a carbon-rich porous material

* Corresponding author.

1944-3994/1944-3986 © 2018 Desalination Publications. All rights reserved.

which is environmentally compatible having excellent stability and cation exchange capacities, high surface area and is easily synthesized from the available raw materials. The proportion of cellulose and lignin components considerably affects the properties of the char which in turn depends on the pyrolysis condition. Therefore, the degree of charring is to be regulated to suit our requirements. The focus of the present work is on the compositional changes occurred during heat-induced transformation (200°C–500°C) in an easily available and abundant agricultural waste, banana stem and its application in the removal of lead from aqueous media.

2. Materials and methods

2.1. Materials

Banana stem, *Musa paradisiaca* L., an abundant agricultural waste, was procured from a field in Kerala. It was properly washed, cut into small pieces, dried, powdered and sieved before the use. For the adsorption studies, $Pb(NO_3)_2$ salt was purchased from E Merck, India. Other reagents such as nitric acid, sodium hydroxide, ammonium hydroxide and sodium sulphide used for the present study were also procured from E Merck, India. The reagents used in the study were all analytical grade reagents.

2.2. Biochar preparation

Banana stem was properly washed, cut into small pieces, dried, powdered and sieved before the use. 10 g of the powdered banana stem was weighed and transferred to silica crucible. The crucible was kept in a preheated muffle furnace, where nitrogen flow was maintained for 15 min continuously. Then the material was charred at 200°C. Different sets of samples were kept for charring at 200°C for different time intervals such as 1, 8, 12, 24, 48 and 72 h. During the process, hemicelluloses undergo limited volatilization and carbonization [8]. Likewise, the biochars were prepared at varying times (1, 8, 12, 24, 48 and 72 h) for the temperatures: 250°C, 300°C, 350°C, 400°C and 500°C. After heating for a specific time and temperature, the crucibles were transferred to nitrogen-filled desiccators. The chars were again powered, sieved and weighed.

2.3. Adsorption experiments

Batch adsorption experiments were carried out on a temperature-controlled water bath shaker set at 200 rpm and maintained at 30°C. The experiments were carried out in a stoppered conical flask (100 mL). The adsorbent selected for all the sorption studies was the biochar prepared at 350°C (12 h). The adsorbent dose was fixed as 2 g L^{-1}.

2.4. Characterization methods

Elemental compositions of the biomass and the char produced at different time and temperature were determined using Vario EL III, Elementar (Kochi, Kerala, India). The oxygen to carbon and hydrogen to carbon atomic ratios were calculated to evaluate the aromaticity of the biochar. Surface morphologies of the biochars were examined using scanning electron micrographs (Philips model XL 30 CP). The surface functionalities in the biochars were characterized by FTIR (Bruker, Germany) scanning from 3,500 to 500 cm^{-1} with a resolution of 2 cm^{-1}. The ^{13}C nuclear magnetic resonance (NMR) of the charred masses was measured using (Bruker Avance III). The surface area, an indicative of porosity and sorption capacity, was determined by Brunauer, Emmett and Teller (BET) analysis (Quantasorb Surface Area Analyzer Qs/7) studying the adsorption of nitrogen at 77 K. X-ray diffraction (XRD) pattern of the biochars was obtained from Rigaku Geigerflex X-ray diffractometer, which enabled to assess the crystallinity and the mineral content of the biochar.

3. Results and discussion

3.1. Characterization of biochars

For the characterization studies, the biochars prepared at 12 h were chosen. As the pyrolysis temperature increases from 200°C to 500°C, the surface area shows an increase from 1.02 to 7.97 m^2 g^{-1} (Table 1). The escape of volatile matters leads to the development of porosity during pyrolysis [14]. The pore diameters obtained indicates that the biochars are mesoporous materials. No appreciable change in surface area is noted as the temperature is raised from 400°C to 500°C. The effect may be because of the formation of stable aromatic carbon structure at higher temperature. Thus greater aromatic character is shown by the chars at higher temperature.

3.1.1. Zero point charge

The point of zero charge of biochars was determined by potentiometric method using the equation:

$$\sigma_0 = \frac{F(C_A - C_B + [OH^-] - [H^+])}{A} \quad (1)$$

where F is the Faraday's constant. C_A and C_B are the concentrations of strong acid or strong base after each addition. $[H^+]$ and $[OH^-]$ are the equilibrium concentrations of H^+ and OH^- ions, respectively (eq/cm^2). A is the surface area of suspension (cm^2 L^{-1}). A graph was plotted (not shown) with σ_0 vs. pH for the biochars. From the point of intersection of σ_0 with the pH curve, the point of zero charge (pH_{zpc}) values were obtained.

The pH_{zpc} on the surface of the biochars was found to be 2.8, 3.1, 3.1, 3.2, 4.0 and 4.6 at 200°C, 250°C, 300°C, 350°C, 400°C and 500°C, respectively. Below the pH_{zpc} surface is

Table 1
BET surface area of the various biochars at 12 h

Temperature (°C)	Surface area (m^2 g^{-1})	Pore diameters (nm)
200	1.02	2.09
250	1.55	2.75
300	5.67	4.45
350	6.03	6.75
400	7.41	6.61
500	7.97	7.10

positive and above the pH_{zpc} surface is negative. The pH_{zpc} value at the highly acidic region, indicating greater negative charge on the surface, may be because of the easy removal of protons from the surface functionalities (carboxylic, sulphonic, phenolic, etc.) on the biochar which imparts a negative charge to the surface [15]. The increase of the pH_{zpc} from 2.8 to 4.6 on increasing the pyrolysis temperature from 200°C to 500°C shows that the surface possesses less negative charge at higher temperatures. This occurs when certain functionalities such as phenolic, carboxylic acids, etc., are lost from the surface [16].

3.1.2. XRD

The XRD patterns of the biochar presented as a function of Bragg's angle given in Fig. 1 reveal the presence of many inorganic crystalline materials in addition to the crystalline cellulosic component. Interplanar spacings of 0.606, 0.533, 0.404 and 0.260 in XRD of 200°C, 250°C and 300°C can be assigned to the crystalline cellulose [1] while the spacings at 0.311 and 0.221 may be attributed to the presence Sylvine (KCl) crystal [17]. As the pyrolysis temperature increases to 350°C, the cellulosic peaks progressively weaken suggesting the decomposition of thermally labile hemicellulose and cellulose. A complete loss of cellulose crystallinity observed at 400°C. On heating to 500°C, signals 0.390–0.370 and 0.209–0.207 indicating turbostratic crystallites, broaden indicating the formation of aromatic units such as phenols, polyaromatic units, heterocyclics [1].

3.1.3. Elemental composition

Elemental composition shows significant changes while charring. Uncharred biomass has 50.9% carbon and 42.1% oxygen. During charring at lower temperatures, the carbon content decrease gradually in the initial hours of heating while oxygen content shows an initial increase and then a decrease [2]. The carbon content loss continues on further heating. At higher temperature (500°C), the carbon loss is found to be rapid on extended heating. Table 2 shows the elemental composition of the biochar at 350°C along with O/C and H/C atomic ratios.

Calculation of oxygen to carbon ratio (Table 2) shows that oxygen to carbon ratio of biochars increase gradually on increasing the heating time at lower temperatures. At higher temperatures also, during the initial hours of heating, a similar trend is observed. The aliphatic carbon is lost rapidly whereas the aromatic carbon formation occurs in the initial hours of charring. As heating proceeds, the loss of aromatic carbon occurs and then remains almost constant with time. The labile oxygen fraction associated with the aliphatic carbon is lost rapidly in the initial hours of charring while the recalcitrant oxygen fraction remains fixed in the char [2]. At higher temperatures, after the initial hours of charring,

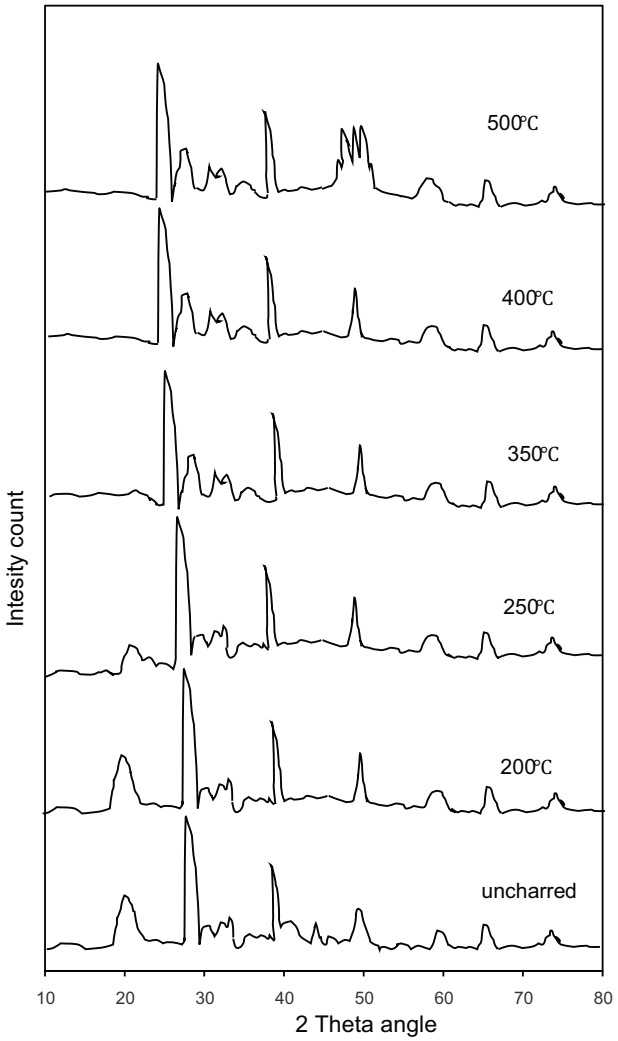

Fig. 1. XRD of uncharred sample and biochars at various temperatures.

Table 2
Elemental composition of the biochar at 350°C along with O/C and H/C atomic ratios

Time (h)	Carbon (%)	Hydrogen (%)	Oxygen (%)	Nitrogen (%)	H/C	O/C
1	75.81	4.56	21.51	0.27	0.722	0.213
8	72.27	4.17	23.45	0.11	0.692	0.243
12	71.11	4.03	24.14	0.13	0.680	0.255
24	71.01	4.00	24.88	0.08	0.676	0.263
36	70.52	3.92	24.97	0.07	0.667	0.266
48	71.4	3.87	24.01	0.07	0.650	0.252
72	70.42	3.76	24.42	0.05	0.641	0.260

the oxygen to carbon ratio is observed to decrease as the heating time is increased and then reach a consistent value. Higher temperature increases the growth of poly-aromatic crystallite clusters which explains greater aromatization and hence greater stability of the biomass on pyrolysis. This is evident from the decrease in the hydrogen to carbon ratios as the heating time is increased [18,19]. The nitrogen content loss observed even at low temperatures may be due to the easy volatilization of nitrogen [8]. Deluca et al. [20] reported that nitrogen begins to volatilize even at a low temperature of 200°C. In addition, at higher temperatures, there is a chance of heterocyclization. There are reports of the presence of recalcitrant heterocyclic nitrogen containing compounds in the biochars [21,22]. During pyrolysis, a series of cleavage and polymerization occur that may result in the creation of thermally stable heterocyclic structures.

The decrease in the O/C ratio with pyrolysis temperature (Table 3) demonstrate that there is a reduction in the biochar surface polar functional groups, making the surface less hydrophilic [23].The charred mass obtained has a higher proportion of carbon in comparison with oxygen. On increasing the heating temperature, the hydrogen to carbon ratio shows an initial decrease which later attains almost a constant value. The changes in the H/C ratios emphasize that aliphatic materials are less resistant to heat treatment than aromatic materials [24].

3.1.4. ^{13}C NMR

The NMR spectrum of biomass and the charred biomass (Fig. 2) indicate that no significant change has occurred during the early hours of pyrolysis. The presence of lignin component imparts aromatic character to the biomass evident from the characteristic peak at 127 ppm. On charring to 350°C for 12 h, it is found that the peaks characteristic of aliphatic carbon due to cellulosic region faded away while the aromatic carbon intensity progressively increased [25]. The characteristic bands observed in the spectra are: 25–45 ppm (alkyl C), 55–70 ppm (aliphatic alcohols), 110–145 ppm (aromatic and unsaturated C), 127 ppm (fused aromatic rings) 145–150 ppm (phenol O-C), 190–210 ppm (carbonyl C) [26]. At lower temperatures, the conversion of aliphatic to aromatic character becomes significant only on increasing the pyrolysis time.

3.1.5. Fourier transform infra-red spectroscopy

A transition of functional groups characteristics of cellulose carbohydrate to aromatic functionality has been observed in the FTIR (Figs. 3 and 4) during the charring. Uncharred biomass shows dominant carbohydrate bands between 1,000 and 1,200 cm^{-1} apart from the aromatic bands. .Aliphatic C–O vibrations correspond to peaks around 1,077 cm^{-1} [27]. The peak at 1,200 cm^{-1} may be attributed to the polysaccharide C–O–C stretch. Aliphatic CH deformations are observed around 1,356 cm^{-1}. On charring, it is found that charred matter is dominated by aromatic functionalities. The peaks around 3,200–3,400 cm^{-1}(O–H stretch) and 2,980–2,850 cm^{-1} (C–H stretch of alkyl functionalities on the surface of the biochar) are destroyed by the pyrolysis to 12 h at 350°C. The destruction of these alkyl functionalities suggest that the biochar surface becomes more and more hydrophobic on extended heating [16,28]. The peaks between 1,650 and 1,700 cm^{-1} indicate C=O stretch due to carboxylic and lactonic acid functionalities [29]. The loss of C=O vibrations and increase in the intensity of aromatic C=C stretching vibrations at 1,491 and 1,560 cm^{-1} describe the extent of charring of the biomass due to pyrolysis at the given time and temperature. Also the aryl C–H vibrations (3,000–3,100 cm^{-1}) progress in intensity on increasing heating time. Aromatic C–O stretching frequencies are also observed at 1,191 and 1,248 cm^{-1} [30].

Table 3
Variation of O/C and H/C ratios with pyrolysis temperatures at 12 h

Temperature (°C)	O/C	H/C
200	0.541	0.875
250	0.501	0.750
300	0.345	0.687
350	0.255	0.680
400	0.212	0.655
500	0.104	0.641

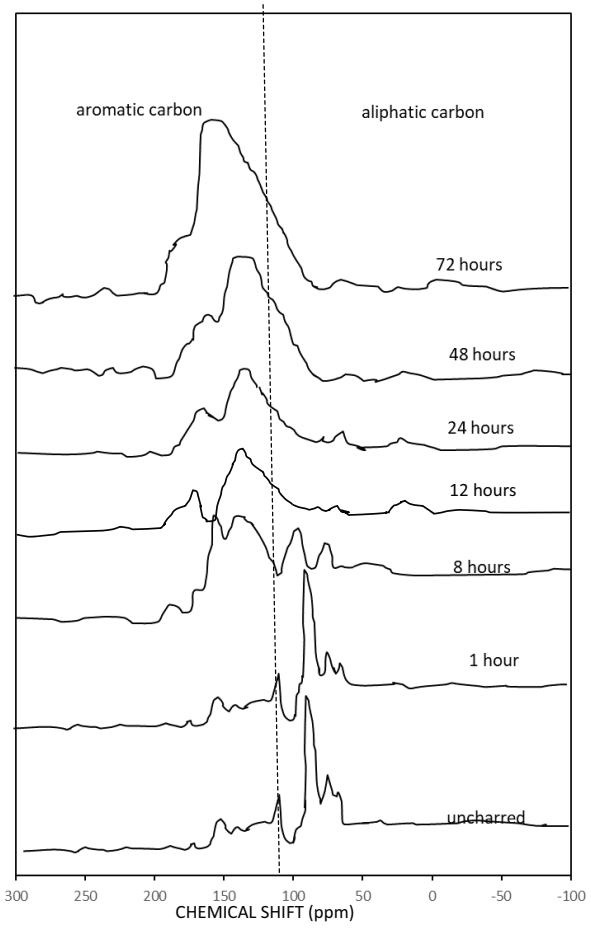

Fig. 2. ^{13}C NMR spectra of banana stem and biochar at 350°C for various times.

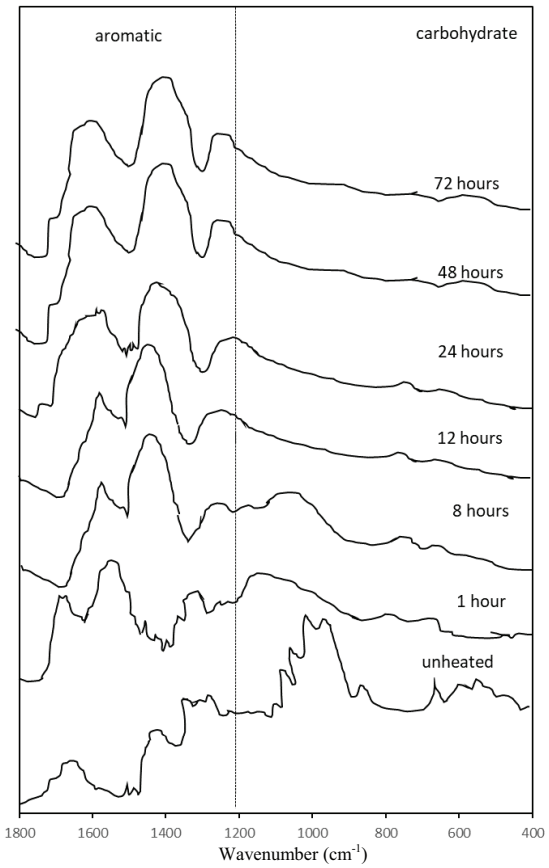

Fig. 3. FTIR spectrum of banana stem at 350°C for various temperatures.

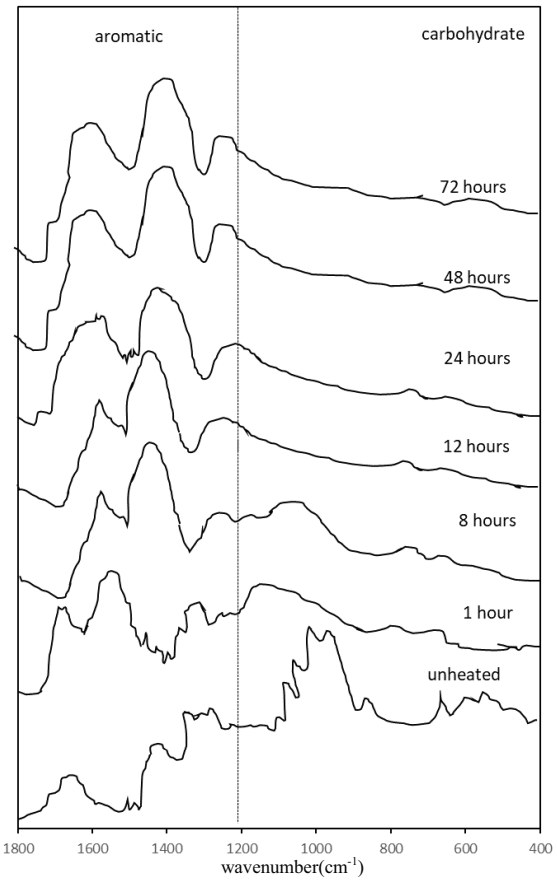

Fig. 4. FTIR spectrum of banana stem at 350°C for various times.

3.1.6. Scanning electron micrographs

Biochar is pyrogenic carbon produced by thermal conversion of lignocellulosic biomass under oxygen free or limited oxygen conditions [31]. Observing SEM images (Fig. 5) of uncharred and charred biomass, it is concluded that smoothening of surface occurred on charring. The biochar surface has a randomly arranged spherical as well as tubular pore structures. Moreover SEM images demonstrate that the pores are finely developed and the pore size distribution is heterogeneous. This indicates the excellent possibility for the various species in aqueous solution to be trapped and adsorbed by the biochars. The fine pore development on the surface of charred mass observed contributed to the surface area of the sample [32]. Therefore, in addition to ion-exchange mechanism and electrostatic interaction, bulk diffusion is also possible on the char surface.

3.2. Effect of solution pH

The sorption of 10 and 25 mg L^{-1} of Pb^{2+} onto the biochar dose of 2 g L^{-1} at different pH varying from 2.0 to 8.0 was studied. It was found that the sorption was very low at 2.0 and 3.0 for both the concentrations. The zero point charge of biochar was found to be 3.2. For pH values 2.0 and 3.0 ($pH < pH_{zpc}$), the adsorbent surface is positively charged. The dominant lead species at the pH values 2.0 and 3.0 is Pb^{2+}. The low sorption percentage observed at pH 2.0 and 3.0 may be because of the electrostatic repulsion between the positively charged adsorbent surface and the Pb^{2+} species. After that, the sorption percentage gradually increased reaching a maximum value of 99.2% and 98.1% for 10 and 25 mg L^{-1} at pH 5.5, respectively. From the speciation diagram [33], after pH 6.0, precipitation of $Pb(OH)_2$ starts which interferes with the adsorption process. From pH value 5.0 to 6.0, the dominant lead species were found to be Pb^{2+} and $Pb(OH)^{+}$. The equilibrium pH lowered after adsorption, indicating the release of H^{+} into the solution. Therefore, the possible mechanism for the sorption was cation exchange mechanism. The polar functional groups such as carboxylic groups on the biochar surface may exchange protons with the cations in the solution. Apart from the cation exchange mechanism, there is a possibility that the electron-rich char surface exerts electrostatic attraction for the cations in the solution. The char surface being porous, an intraparticle diffusion of cations may occur which get trapped very well in these pores.

3.3. Effect of adsorbent dose

The removal efficiency of Pb^{2+} with an initial concentration of 100 mg L^{-1} was studied at 30°C increasing the adsorbent dose from 2 to 8 g L^{-1}. The adsorbent percentage increased from 82% to 95.3% as the adsorbent dose increased from 2 to 8 g L^{-1}. This may be attributed to the exposure of

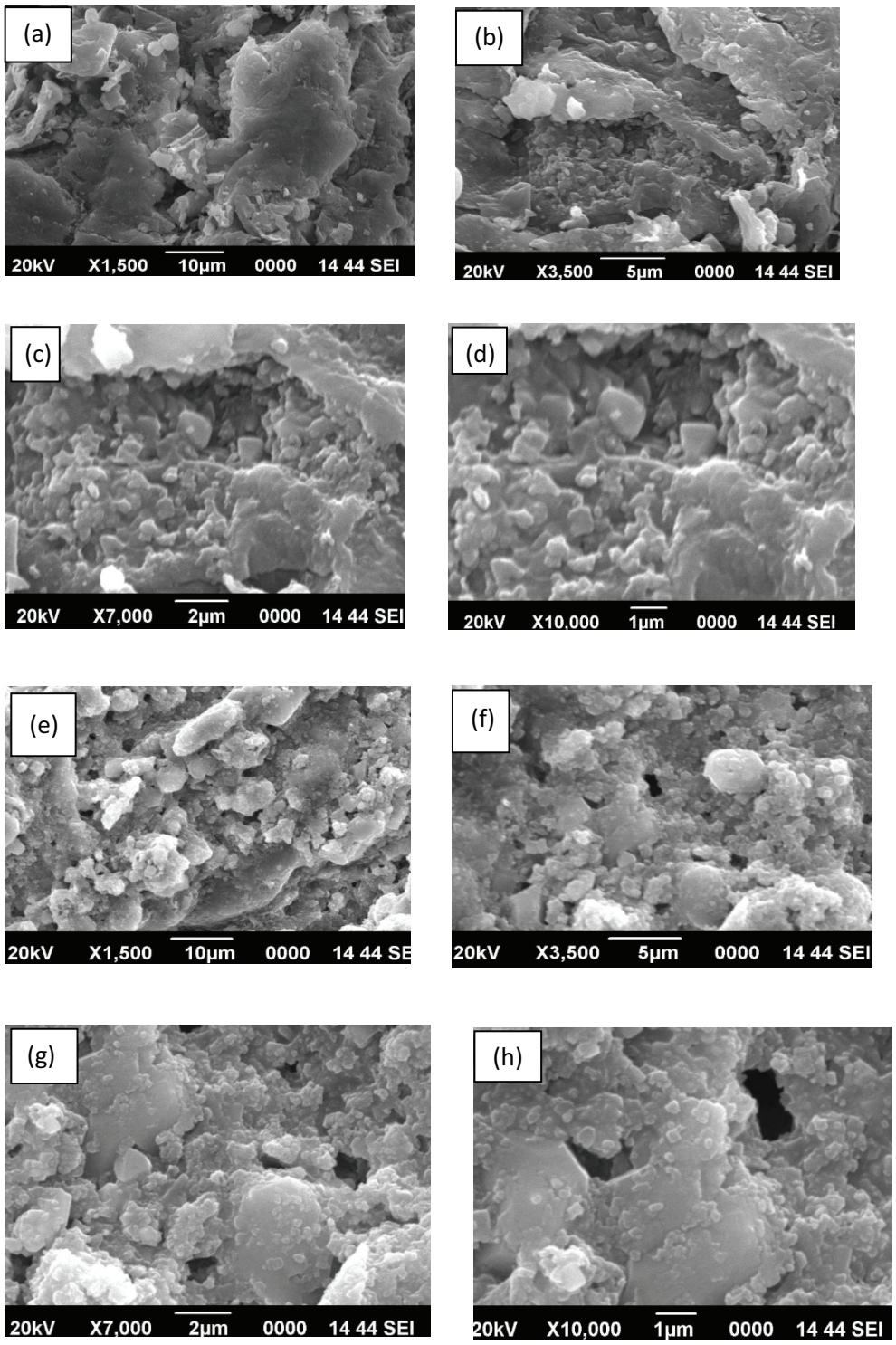

Fig. 5. SEM photograph of banana stem: (a)–(d) indicate images of uncharred sample and (e)–(h) indicate images of charred sample at 350°C.

more sorption surface and the availability of more sorption sites. But the amount adsorbed showed a variation from 37.4 to 11.9 mg g^{-1}, respectively. This indicates that it is effective to carry out the adsorption with 2 g L^{-1} sorbent dose than with higher dosages (Table 4).

3.4. Adsorption kinetics

The adsorption of Pb^{2+} as a function of time and concentration was studied. 10 and 25 mg L^{-1} of the Pb^{2+} solutions were taken for the study using biochar as the sorbent.

1 mL of the solution was taken after regular time intervals (1, 5, 10, 30, 60, 90 and 120 min). The concentrations were determined using UV-visible spectrophotometer (λ_{max}). After 120 min, the adsorption percentage was found to be a constant for both 10 and 25 mg L^{-1}. Therefore, the equilibrium time was fixed as 120 min. The data obtained were fitted to:

(a) Pseudo – first order

$$\text{kinetic model: } \log(q_e - q_t) = \log q_e - \frac{k_1}{2.303}t \quad (2)$$

and

(b) Pseudo-second order

$$\text{kinetic model: } \frac{1}{q_t} = \frac{1}{k_2 q_e^2 t} + \frac{1}{q_e} \quad (3)$$

where k_1 is the pseudo-first order rate constant of adsorption and k_2 is the pseudo-second-order rate constant of adsorption and q_e and q_t are the amounts of metal ions sorbed at equilibrium and at time t, respectively.

The correlation co-efficient for the pseudo-first-order kinetic equation is found to be higher than that of the pseudo-second order indicating that the pseudo-first order kinetics is the best fit model. This implies that the rate determining step involves physical adsorption and the solute uptake rate is directly proportional to the ratio of solute concentration and the amount of adsorbent. The parameters of kinetics are shown in Table 5.

Table 4
Effect of adsorbent dose on the adsorption of 100 mg L^{-1} Pb(II) solution

Adsorbent dose (g L^{-1})	Adsorption (%)	Amount adsorbed (mg g^{-1})
2	74.0	37.4
4	88.4	22.1
6	93.2	15.5
8	95.3	11.9

3.5. Adsorption isotherms

The sorption onto the biochar is influenced by the structural and chemical properties of the sorbent surface as well as the sorbate. Adsorption also depends on the pore size distribution, specific surface area, polarity and functionality of the biochar surface. A better understanding of the sorbent–sorbate interaction is made possible from the isotherm studies. The varying concentrations 10, 25, 50, 100, 200 and 300 mg L^{-1} of Pb^{2+} were chosen for the isotherm study. The calculated isotherm parameters are given in Table 6. The sorption data obtained were interpreted using Langmuir and Freundlich isotherm models:

$$\text{Langmuir isotherm: } \frac{C_e}{q_e} = \frac{1}{Q^0 b} + \frac{C_e}{Q^0} \quad (4)$$

where q_e and C_e are the equilibrium concentration of Pb^{2+} onto the biochar and in solution, respectively. Q^0 and b are Langmuir constants related to adsorption capacity and energy of adsorption, respectively.

$$\text{Freundlich isotherm: } \log q_e = \log K_F + \frac{1}{n}\log C_e \quad (5)$$

where K_F and $1/n$ are the Freundlich constants related to adsorption capacity and intensity of adsorption, respectively.

The sorption data fitted very well with the Freundlich model with high regression co-efficient. The Freundlich constant, $1/n$, is found to be less than 1, suggesting that

Table 6
Isotherm parameters for the adsorption of Pb(II) onto biochar

Isotherm constants	Pb^{2+}
Freundlich	
K_F	11.88
$1/n$	0.38
R^2	0.996
Langmuir	
Q^0 (mg g^{-1})	140.8
b	0.05
R^2	0.957

Table 5
kinetic parameters

Pseudo-first order kinetic model				
Pb^{2+} concentration (mg L^{-1})	k_1 (min^{-1})	q_e exp (mg g^{-1})	q_e cal (mg g^{-1})	R^2
10	0.153	4.95	4.77	0.9991
25	0.161	12.18	11.92	0.9980
Pseudo-second order kinetic model				
Pb^{2+} concentration (mg L^{-1})	$k_2 \times 10^{-3}$ (g mg^{-1} min^{-1})	q_e exp (mg g^{-1})	q_e cal (mg g^{-1})	R^2
10	7.112	4.95	2.79	0.9612
25	3.365	12.18	8.10	0.9120

the adsorption sites on the biochar are not homogeneous. The adsorption behavior is multilayer adsorption which involves physical adsorption, which confirms the data obtained from the kinetic studies.

4. Conclusion

Banana stem was used for the biochar production at different temperatures. The various complex changes that occurred in the process were monitored using characterization techniques such as NMR, FTIR, XRD and elemental composition determination. After 12 h charring at 350°C, aromatic functional groups showed dominance as evident from FTIR and NMR. At higher temperatures, the speed of conversion of aliphatic functionality to aromatic functionality was found to be greater. This means that the formation conditions profoundly influenced the char functionality. Taking advantage of the surface structure and functionalities of the biochar, the kinetic and isotherm studies of the adsorption of Pb(II) onto the biochar was conducted. The optimum pH for the adsorption of Pb(II) was found to be 5.5. The variation in the amount adsorbed from 37.4 to 11.9 mg g^{-1}, respectively, indicates that it is effective to carry out the adsorption with 2 g L^{-1} sorbent dose than with higher dosages. The kinetic data obtained fitted very well to the pseudo-first order model indicating that the rate determining step involved physical adsorption and the solute uptake rate was directly proportional to the ratio of solute concentration and the amount of adsorbent. The regression coefficient was found to be higher for Freundlich isotherm model, suggesting that the adsorption sites on the biochar were not homogeneous.

Acknowledgements

The authors would like to express their sincere gratitude to the Head, Department of Chemistry, Fatima Mata National College, Kollam, for providing laboratory facilities. N.B. Fernandez would like to thank UGC, New Delhi, for financial assistance in the form of Minor Research Project (2326-MRP/15-16/KLKE015/UGC-SWRO). Jelen Das Y greatly acknowledges KSCSTE, Government of Kerala, for financial assistance in the form of Student Project Scheme (2017/KSCSTE84/SPS61). The authors would like to sincerely acknowledge the services rendered by Indian Institute of Science, Bangalore, for their assistance in the characterization of the samples.

References

[1] M. Keiluweit, P.S. Nico, M.G. Johnson, M. Kleber, Dynamic molecular structure of plant biomass-derived black carbon(biochar), Environ. Sci. Technol., 44 (2010) 1247–1253.
[2] D.W. Rutherford, R.L. Wershaw, C.E. Rostad, C.N. Kelly, Effect of formation condition on biochars: compositional and structural properties of cellulose, lignin, and pine biochars, Biomass Bioenergy, 46 (2012) 693–701.
[3] U. Uras, M. Carrier, A.G. Hardie, J.H. Knoetze, Physiochemical characterization of biochars from vacuum pyrolysis of south African agricultural waste for application as soil amendments, J. Anal. Appl. Pyrolysis, 98 (2012) 207–213.
[4] D. Savova, E. Apak, E. Ekinci, F. Yardim, N. Petrov, T. Budinova, M. Razvigorova, V. Minkova, Biomass conversion to carbon adsorbents and gas, Biomass Bioenergy, 21 (2001) 133–142.
[5] D. Mohan, S. Rajput, V.K. Singh, P.H. Steele, C.U. Pittman, Jr., Modeling and evaluation of chromium remediation from water using a low cost bio-char, a green adsorbent, J. Hazard. Mater., 188 (2011) 319.
[6] N.N. Nassar, Rapid removal and recovery of Pb(II) from wastewater by magnetic nanoadsorbents, J. Hazard. Mater., 184 (2010) 538–546.
[7] X.F. Tan, Y.G. Liu, G. Zeng, X. Wang, X. Hu, Y. Gu, Z. Yang, Application of biochar for the removal of pollutants from aqueous solutions, Chemosphere, 125 (2015) 70–85.
[8] X. Cao, W. Harris, Properties of dairy-manure-derived biochar pertinent to its potential use in remediation, Bioresour. Technol., 101 (2010) 5222–5228.
[9] E. Suganya, S. Rangabhashiyam, A.V. Lity, N. Selvaraju, Removal of hexavalent chromium from aqueous solution by a novel biosorbent *Caryota urens* seeds: equilibrium and kinetic studies, Desal. Wat. Treat., 57 (2016) 1–11.
[10] M.T. Amin, A.A. Alazba, M. Shafiq, Adsorption of copper (Cu^{2+}) from aqueous solution using date palm trunk fibre: isotherms and kinetics, Desal. Wat. Treat., 57 (2016) 1–13.
[11] F.S. Hashem, M.S. Amin, Adsorption of methylene blue by activated carbon derived from various fruit peels, Desal. Wat. Treat., 57 (2016) 1–12.
[12] Z.-P. Qi, Q. Liu, Z.-R. Zhu, Q. Kong, Q.-F. Chen, C.-S. Zhao, Y.-Z. Liu, M.-S. Miao, C. Wang, Rhodamine B removal from aqueous solutions using loofah sponge and activated carbon prepared from loofah sponge, Desal. Wat. Treat., 57 (2016) 1–13.
[13] G.E. Sharaf El-Deena, S.E.A. Sharaf El-Deen, Kinetic and isotherm studies for adsorption of Pb(II) from aqueous solution onto coconut shell activated carbon, Desal. Wat. Treat., 57 (2016) 1–22.
[14] W. Yang, F. Zheng, Y. Lu, X. Xue, N. Li, Adsorption interaction of tetracyclines with porous synthetic resins, Ind. Eng. Chem., 50 (2011) 13892–13898.
[15] J.M. Novak, W.J. Busscher, D.L. Laird, M. Ahmedna, D.W. Watts, M.A.S. Niandou, Impact of biochar amendment on fertility of a southern coastal plain soil, Soil Sci., 174 (2009) 105–112.
[16] T.J. Kinney, C.A. Masiello, B. Dugan, W.C. Hockaday, M.R. Dean, K. Zygourakis, R.T. Barnes, Hydrologic properties of biochars produced at different temperatures, Biomass Bioenergy, 41 (2012) 34–43.
[17] A. Silber, I. Levkovitch, E.R. Graber, PH-dependent mineral release and surface properties of cornstraw biochar: agronomic implication, Environ. Sci. Technol., 44 (2010) 9318–9323.
[18] A.V. Mc Beath, R.J. Smernik, Variation in degree of aromatic condensation of chars, Org. Geochem., 40 (2009) 1161–1168.
[19] R.A. Brown, A.K. Kercher, T.H. Nguyen, D.C. Nagle, W.P. Ball, Production and characterisation of synthetic wood chars for use as surrogates for natural sorbents, Org. Geochem., 37 (2006) 321–333.
[20] T.H. Deluca, M.D. Mackenzie, M.J. Gundale, Biochar Effect on Soil Nutrient Transformation, J. Lehmann, S. Joseph, Eds., Biochar for Environmental Management: Science and Technology, Earthscan, London, 2009, pp. 251–270.
[21] S. Koutcheiko, C.M. Monreal, H. Kodama, T. Mc Cracken, L. Kotlyar, Preparation and characterization of activated carbon derived from the thermos-chemical conversion of chicken manure, Bioresour. Technol., 98 (2007) 2459–2464.
[22] K.B. Cantrell, P.G. Hunt, M. Uchimiya, J.M. Novak, Impact of pyrolysis temperature and manure source on physicochemical characteristics of biochar, Bioresour. Technol., 107 (2012) 419–428.
[23] M. Ahmad, S.S. Lee, X. Dou, D. Mohan, J.R. Sung, J.E. Yang, Y.S. Ok, Effect of pyrolysis temperature on soybean stover- and peanut shell-derived biochar properties and TCE adsorption in water, Bioresour. Technol., 118 (2012) 536–544.
[24] C. Amen-Chen, H. Pakdel, C. Roy, Production of monomeric phenols by thermochemical conversion of biomass-a review, Bioresour. Technol., 79 (2001) 277–299.
[25] P.L. Ascough, M.I. Bird, P. Wormald, C.E. Snape, D. Apperley, Influence of production variables and starting material on charcoal stable isotopic and molecular characteristics, Geochim. Acta, 72 (2008) 6090–6102.

[26] F.J. Gonzalez-Vila, P. Tinoco, G. Almendros, F. Martin, Pyrolysis-GC-MS analysis of the formation and degradation stages of charred residues from lignocellulosic biomass, J. Agric. Food Chem., 49 (2001) 1128–1131.
[27] C. Trigo, L. Cox, K. Spokas, Influence of pyrolysis temperature and hardwood species on resulting biochar properties and their effect on azimsulfuron sorption as compared to other sorbents, Sci. Total Environ., 566–567 (2016) 1454–1464.
[28] M. Tatzber, M. Stemmer, H. Spiegel, C. Katzlberger, G. Zehetner, G. Haberauer, E. Garcia-Garcia, M.H. Gerzabeck, Spectroscopic behaviour of ^{14}C labeled humic acids in a long term field experiment with three cropping systems, Aust. J. Soil Res., 47 (2009) 459–469.
[29] R.K. Sharma, J.B. Wooten, V.L. Baliga, X. Lin, W. Geoffrey Chan, M.R. Hajaligol, Characterization of chars from pyrolysis of lignin, Fuel, 83 (2004) 1469–1482.
[30] T. Mimmo, P. Panzacchi, M. Baratieri, C.A. Davies, G. Tonon, Effect of pyrolysis temperature on Miscanthus (Miscanthus × giganteus) biochar physical, chemical and functional properties, Biomass Bioenergy, 62 (2014) 149–157.
[31] J. Lehmann, J. Gaunt, M. Rondon, Biochar sequestration in terrestrial eco systems-a review, Mitigation Adapt. Strategies Global Change, 11 (2006) 403–427.
[32] P. Sun, C. Hui, R. Azim Khan, J. Du, Q. Zhang, Y.H. Zhao, Efficient removal of crystal violet using Fe_3O_4-coated biochar: the role of the Fe_3O_4 nano particles and modeling study their adsorption behaviour, Sci. Rep., 5 (2015) 12638.
[33] G. Wulfsberg, Inorganic Chemistry: Effect of Concentration and pH on Redox Chemistry: Pourbaix Diagram, University Science Books, Vol. 4, 2014, pp. 287–289.